

Low-Energy Supernova Constraints on Lepton Flavor Violating Axions

Zi-Miao Huang,^a Zuwei Liu^a

^a*Department of Physics, Nanjing University, Nanjing 210093, China*

E-mail: zimiaohuang@smail.nju.edu.cn, zuweiliu@nju.edu.cn

ABSTRACT: The extreme conditions within the supernova core, a high-temperature and high-density environment, create an ideal laboratory for the search for new physics beyond the Standard Model. Of particular interest are low-energy supernovae, characterized by their low explosion energies, which place strong constraints on the new-physics energy transfer from the core to the mantle. We compute low-energy supernova constraints on lepton-flavor-violating axions and axion-like particles that couple to both electrons and muons. For axion mass above the muon mass, the electron-muon coalescence and the axion decay are dominant production and reabsorption processes, respectively. We find that the low-energy supernovae provide the most stringent constraints on the axions in the mass range of $\sim (110, 550)$ MeV, probing the coupling constant down to $g_{ae\mu} \simeq \mathcal{O}(10^{-11})$.

Contents

1	Introduction	1
2	ALP model	2
3	Energy deposition	2
4	ALP production and absorption	3
5	Results	7
6	Conclusion	8

1 Introduction

Axions are hypothetical particles proposed to resolve the strong CP problem in quantum chromodynamics [1–4]. Beyond the original axion, a broader class of pseudo-scalar particles, commonly referred to as axion-like particles (ALPs), emerges naturally in many well-motivated extensions of the Standard Model (SM) [5–8]. A particularly intriguing subclass of ALPs comprises those that exhibit lepton-flavor-violating (LFV) couplings to SM particles [6, 7, 9–16]. We will use “axion” and “ALP” interchangeably in this paper. The most stringent bounds on LFV ALPs with masses above the GeV scale arise from accelerator-based searches [17–25]. In the sub-GeV mass regime, the leading bounds come from rare decay experiments [26–39], as well as astrophysical observations [35, 40, 41].

Recently, the supernova (SN) cooling bounds on LFV ALPs that couple to electrons and muons have been investigated in Refs. [35, 40, 41]. In this work, we extend the analysis by considering constraints from low-energy supernovae (LESNe), a subclass of underluminous Type II-P SNe, which are typically 10 to 100 times dimmer than ordinary core-collapse SNe (CCSNe). LESNe have been identified in both astronomical observations [42–52] and SN simulations [53–61]. LESNe can have an explosion energy as low as $0.1 B = 10^{50}$ erg, which has been found both in astronomical observations and in simulations [50]. For example, the reconstructed explosion energy of SN 1054 is found to be around 0.1 B or less [47, 60, 62]. In contrast to the conventional cooling bounds, which require the energy loss from new physics to be less efficient than that from neutrinos [63], the LESN constraints arise from the requirement that energy deposited in the SN mantle by new particles must remain below the LESN explosion energy, 0.1 B [62, 64, 65]. Recent studies have demonstrated that LESNe can place powerful limits on a broad class of new physics scenarios [62, 66–73].

For LFV ALPs that couple to electrons and muons and have masses below ~ 100 MeV, the leading constraints come from rare muon decay experiments [26, 27, 29, 30, 33]. For LFV ALPs with masses above ~ 100 MeV, one of the leading constraints comes from the

SN cooling bounds [41]. The axion production channels inside the SN core include muon decay [35], axion bremsstrahlung [40], and electron-muon coalescence [41]. For LFV ALPs with masses above ~ 100 MeV, the dominant axion production channel in the SN core is the electron-muon coalescence process [41]. In this work, we focus on ALPs with masses above ~ 100 MeV and study the LESN constraints. By requiring that the energy deposition in the SN mantle through ALP decay to be less than the LESN explosion energy 0.1 B, we derive constraints for ALP masses in the range $m_a \sim (110, 550)$ MeV. We find that the LESN constraints probe new parameter space that is unconstrained by the SN cooling limits derived in Ref. [41].

The rest of the paper is organized as follows. In section 2, we introduce the LFV ALP model. In section 3, we analyze the energy deposition in the SN mantle induced by ALPs produced in the SN core. In section 4, we evaluate the ALP production and absorption rates. We present and discuss our results in section 5, and summarize our main findings in section 6.

2 ALP model

We consider LFV ALPs that couple to electrons and muons via the following interaction Lagrangian:

$$\mathcal{L}_{\text{int}} = \frac{g_{ae\mu}}{m_e^0 + m_\mu} \bar{e} \gamma^\lambda \gamma_5 \mu \partial_\lambda a + \text{h.c.}, \quad (2.1)$$

where a is the ALP field, e is the electron field, μ is the muon field, $m_e^0 = 0.511$ MeV is the electron mass in vacuum, and $m_\mu = 105.6$ MeV is the muon mass. The interaction Lagrangian given in Eq. (2.1) is equivalent to the following interaction

$$\mathcal{L}_{\text{int}} = -ig_{ae\mu} a \bar{e} \gamma_5 \mu + \text{h.c.}, \quad (2.2)$$

if the fermions are on-shell [41, 74–76]. In this work, we use Eq. (2.2) to compute the ALP production and reabsorption rates in the SN analysis.

3 Energy deposition

LFV ALPs can be copiously produced in the SN core and subsequently reabsorbed in the SN mantle, leading to energy deposition in the mantle, which contributes to the SN explosion energy. Thus, to compute the LESN constraints, we first compute the energy deposition in the SN mantle caused by the reabsorption of ALPs [62]:

$$E_m = \Delta t \int_0^{R_{\text{NS}}} dr \int_{m'_a(r)}^\infty dE_a \frac{dL_a(r, E_a, t)}{dr dE_a} \left[\exp\left(\frac{r - R_{\text{NS}}}{\lambda_a(r)}\right) - \exp\left(\frac{r - R_*}{\lambda_a(r)}\right) \right], \quad (3.1)$$

where $\Delta t = 3$ seconds is the typical SN explosion duration, R_{NS} is the core radius, R_* is the radius of the progenitor star, $m'_a = m_a/\text{lapse}(r)$, which encodes gravitational redshift effects on the ALP mass m_a through the lapse factor $\text{lapse}(r)$ [62], $L_a(r, E_a, t)$ is the ALP luminosity with energy E_a at radial coordinate r and time t , and $\lambda_a(r) = v_a/\Gamma_a$ is the ALP

mean free path with $v_a = \sqrt{E_a^2 - m_a^2}/E_a$ and Γ_a being the ALP velocity and decay width in the SN frame, respectively.

In our analysis, we use $R_{\text{NS}} = 20$ km and $R_* = 3 \times 10^7$ km. Because typically R_* is in the range of $\simeq (3 - 50) \times 10^7$ km [62], our choice represents a conservative estimate of the constraint. The ALP luminosity is computed via

$$\frac{dL_a(r, E_a, t)}{dr dE_a} = 4\pi r^2 \text{lapse}(r)^2 (1 + 2v_r) E_a \frac{d^2 n_a}{dt dE_a}, \quad (3.2)$$

where $d^2 n_a / dt dE_a$ is the ALP production rate per unit volume and per unit energy, and v_r is the velocity of the emitting medium in the radial direction. Because $v_r \ll 1$ [62], we neglect it in our analysis.

4 ALP production and absorption

In this work, we focus on LFV ALPs with masses $m_a > m_\mu + m_e$. In general, LFV ALPs can be produced in the SN core via the following channels: muon decay, axion bremsstrahlung, and electron-muon coalescence [41]. For $m_a > m_\mu + m_e$, the dominant production channel is the electron-muon coalescence process [41]. Thus, in our analysis, we consider only ALP production through the electron-muon coalescence process, and neglect the muon decay and axion bremsstrahlung processes. For ALP reabsorption, we consider only the leading effects from the ALP decay process in this mass regime.

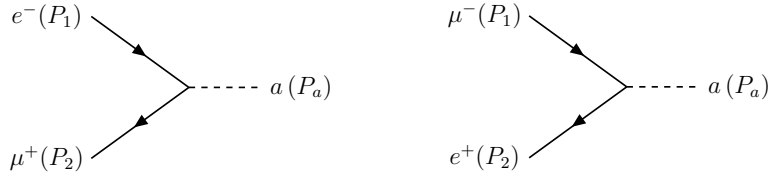


Figure 1. The electron-muon coalescence processes for the ALP production: $e^- + \mu^+ \rightarrow a$ (left) and $\mu^- + e^+ \rightarrow a$ (right).

Fig. 1 shows the two Feynman diagrams for the electron-muon coalescence process: $e^- + \mu^+ \rightarrow a$ and $\mu^- + e^+ \rightarrow a$. The ALP production rate for $\mu^- + e^+ \rightarrow a$ is given by [41]

$$\frac{d^2 n_a}{dt dE_a} (\mu^- + e^+ \rightarrow a) = \frac{|\mathcal{M}_c|^2}{32\pi^3} \int_{E_2^-}^{E_2^+} dE_2 f_\mu^- f_e^+, \quad (4.1)$$

where $|\mathcal{M}_c|^2 = 2g_{ae\mu}^2 [m_a^2 - (m_\mu - m_e)^2]$, f_i^\mp is the Fermi-Dirac distribution for fermion (antifermion) i :

$$f_i^\mp = \left[e^{(E_i \mp \mu_i)/T} + 1 \right]^{-1}, \quad i = e, \mu. \quad (4.2)$$

The upper and lower limits for the integral in Eq. (4.1) are

$$E_2^\pm = \frac{E_a(m_a^2 - m_1^2 + m_2^2)}{2m_a^2} \pm \frac{\sqrt{E_a^2 - m_a^2}}{2m_a^2} I, \quad (4.3)$$

where m_1 (m_2) is the fermion (antifermion) mass and

$$I = \sqrt{(m_1^2 - m_2^2 - m_a^2)^2 - 4m_2^2 m_a^2}. \quad (4.4)$$

For the ALP production rate in the $e^- + \mu^+ \rightarrow a$ process, one changes $f_\mu^- f_e^+$ to $f_e^- f_\mu^+$ in Eq. (4.1):

$$\frac{d^2 n_a}{dt dE_a}(e^- + \mu^+ \rightarrow a) = \frac{|\mathcal{M}_c|^2}{32\pi^3} \int_{E_2^-}^{E_2^+} dE_2 f_e^- f_\mu^+. \quad (4.5)$$

Note that for both $\mu^- + e^+ \rightarrow a$ and $e^- + \mu^+ \rightarrow a$ processes, P_1 and P_2 denote the four-momenta of the initial state particle and anti-particle, respectively.

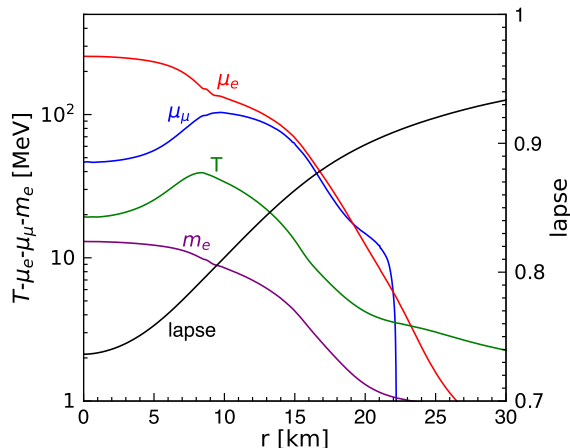


Figure 2. The Garching profiles for the SFHo-18.8 SN model at 1 second postbounce [77]: temperature T , the electron chemical potential μ_e , the muon chemical potential μ_μ , the gravitational lapse factor, and the in-medium electron mass m_e computed via Eq. (4.6).

To study LESN constraints, we follow Ref. [62] to adopt the Garching muonic model SFHo-18.8 [77, 78], the coldest model presented in Ref. [78]. The SFHo-18.8 model has a peak temperature of 30-40 MeV and a final neutron star mass of $1.351 M_\odot$ (baryonic) and $1.241 M_\odot$ (gravitational) [62], which are compatible with predictions by theoretical models for LESNe [53–56, 58–61, 79–81]. Because the neutron star mass of the SFHo-18.8 model is close to the minimal neutron star mass expected in CCSNe [62], constraints derived with this model can be regarded as conservative estimates of LESN bounds. Fig. 2 shows various profiles from the SFHo-18.8 model at 1 second postbounce, including temperature T , electron chemical potential μ_e , muon chemical potential μ_μ , and the gravitational lapse factor. To accurately compute the ALP production rate via electron-muon coalescence and the ALP absorption rate via its inverse process, we use the in-medium electron mass, which receives significant corrections due to plasma effects in the SN core [75, 82]:

$$m_e = \frac{m_e^0}{\sqrt{2}} + \sqrt{\frac{(m_e^0)^2}{2} + \frac{\alpha}{\pi}(\mu_e^2 + \pi^2 T^2)}, \quad (4.6)$$

where $\alpha = 1/137$ is the fine-structure constant. We note that Eq. (4.6) is an approximate expression, valid in the ultra-relativistic limit, which is appropriate for the SN analysis

in this study. We obtain the radial distribution of the in-medium electron mass m_e , by using the SN profiles of temperature T and electron chemical potential μ_e . The in-medium electron mass is found to decrease significantly from ~ 12.9 MeV at the core center ($r = 0$) to ~ 1.3 MeV at $r = 20$ km, as shown in Fig. 2.

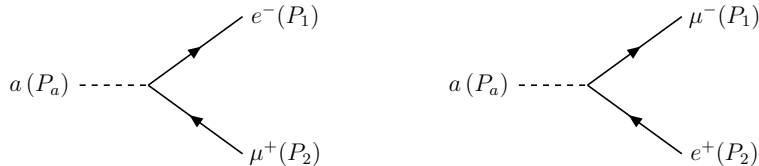


Figure 3. The ALP decay processes: $a \rightarrow e^- + \mu^+$ (left) and $a \rightarrow \mu^- + e^+$ (right).

We next compute the ALP absorption rate. For heavy ALPs with masses $m_a > m_\mu + m_e$, the dominant reabsorption processes are the ALP decay processes, $a \rightarrow e^\pm + \mu^\mp$, as shown in Fig. 3, which are the inverse of the processes shown in Fig. 1. The absorption rate for the process of $a \rightarrow f$ is related to the production rate via [41]

$$\Gamma_{a \rightarrow f}(E_a) = e^{(E_a - \mu_{a \rightarrow f}^0)/T} \frac{2\pi^2}{|\mathbf{p}_a| E_a} \frac{d^2 n_a}{dt dE_a}, \quad (4.7)$$

where $|\mathbf{p}_a| = \sqrt{E_a^2 - m_a^2}$, $d^2 n_a / dt dE_a$ is the production rate for the corresponding electron-muon coalescence process, and $\mu_{a \rightarrow f}^0 = \sum_p \mu_p$ with μ_p denoting the chemical potential of the particle p in the final state. Thus, one has $\mu_{a \rightarrow e^- + \mu^+}^0 = \mu_e - \mu_\mu$ for the process of $a \rightarrow e^- + \mu^+$, and $\mu_{a \rightarrow \mu^- + e^+}^0 = \mu_\mu - \mu_e$ for the process of $a \rightarrow \mu^- + e^+$, where μ_e (μ_μ) denotes the electron (muon) chemical potential. We note that in regions where the ALP is in equilibrium, $\mu_{a \rightarrow f}^0$ becomes the chemical potential of the ALP and thus vanishes. In such cases, the electron chemical potential should be equal to the muon chemical potential, and one can no longer use the Garching profiles where the electron chemical potential is significantly different from the muon chemical potential. Equilibrium between the ALP and SM particles can be achieved in regions of parameter space where the coupling strength is sufficiently large. A detailed analysis of such cases will be presented in a future study [83].

Fig. 4 shows the ALP production rates for the two electron-muon coalescence processes shown in Fig. 1, and the absorption rates for the two ALP decay processes shown in Fig. 3, as a function of the radius r , for the benchmark model point: $(E_a, m_a, g_{ae\mu}) = (250 \text{ MeV}, 200 \text{ MeV}, 1.4 \times 10^{-11})$. For $10 \lesssim r \lesssim 22$ km, the two electron-muon coalescence processes yield similar production rates; for $r \lesssim 10$ km and $r \gtrsim 22$ km, the $e^- + \mu^+ \rightarrow a$ process has a larger production rate than the $\mu^- + e^+ \rightarrow a$ process. To understand this behavior, we compute the number density

$$n_{\ell^\mp}(r) = \frac{1}{\pi^2} \int_0^\infty dp p^2 f_\ell^\mp(r), \quad \ell = e, \mu, \quad (4.8)$$

where f_ℓ^\mp is given in Eq. (4.2). As shown in the right panel of Fig. 5, in the $r \lesssim 10$ km region we have $n_{e^-} > n_{\mu^-}$ and $n_{\mu^+} > n_{e^+}$, while in the $r \gtrsim 22$ km region we have $n_{e^-} > n_{e^+}$

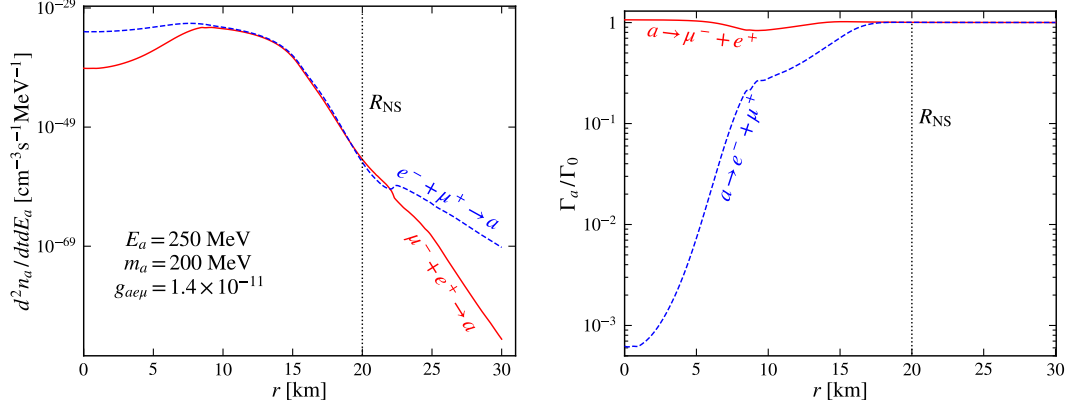


Figure 4. **Left panel:** ALP production rate as a function of the radius r in $e^- + \mu^+ \rightarrow a$ (blue dashed) and $\mu^- + e^+ \rightarrow a$ (red solid). **Right panel:** ALP absorption rate (normalized to its vacuum value, Γ_0) as function of radius r for $a \rightarrow e^- + \mu^+$ (blue dashed) and $a \rightarrow \mu^- + e^+$ (red solid). For both panels, we use $E_a = 250$ MeV, $m_a = 200$ MeV, and $g_{ae\mu} = 1.4 \times 10^{-11}$. $R_{\text{NS}} = 20$ km is the neutron star core radius (black dotted).

and $n_{\mu^+} > n_{\mu^-}$. Therefore, in both regions, $n_{e^-} n_{\mu^+} > n_{\mu^-} n_{e^+}$, which explains why the $e^- + \mu^+ \rightarrow a$ channel dominates over the $\mu^- + e^+ \rightarrow a$ channel there. Note that $n_{\mu^+} > n_{\mu^-}$ in the $r \gtrsim 22$ km region arises because the muon chemical potential becomes negative in that region, as shown in the left panel of Fig. 5.

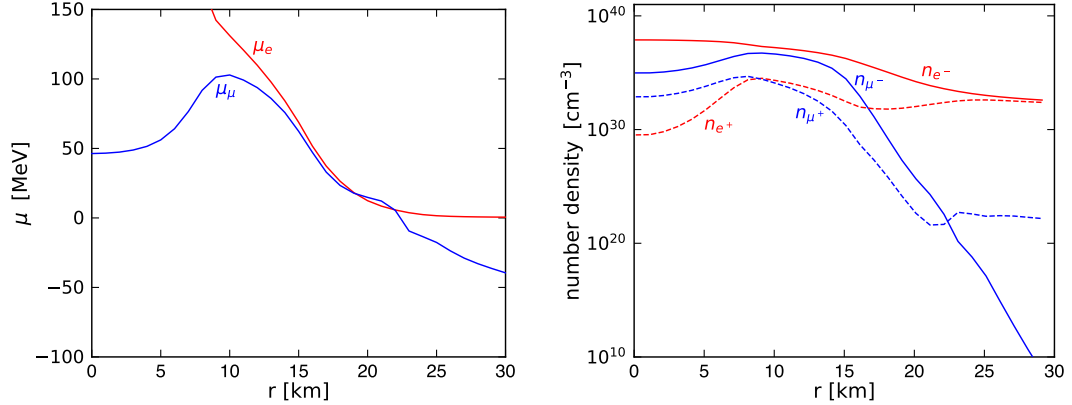


Figure 5. **Left panel:** Electron chemical potential μ_e (red) and muon chemical potential μ_μ (blue) from the SFHo-18.8 model profiles [77]. **Right panel:** Number densities of e^- (red-solid), μ^- (blue-solid), e^+ (red-dashed), and μ^+ (blue-dashed) calculated using Eq. (4.8).

The ALP absorption rates shown in Fig. 4 are normalized to the decay width in the vacuum, Γ_0 , which is

$$\Gamma_0 = \frac{g_{ae\mu}^2}{8\pi E_a m_a^2} [m_a^2 - (m_\mu - m_e^0)^2] \sqrt{(m_\mu^2 - (m_e^0)^2 - m_a^2)^2 - 4(m_e^0)^2 m_a^2}. \quad (4.9)$$

For $r \lesssim 15$ km, the decay channel $a \rightarrow \mu^- + e^+$ dominates over $a \rightarrow e^- + \mu^+$. This pronounced disparity arises primarily from the exponential factor in Eq. (4.7). At these

radii, the electron chemical potential μ_e is significantly larger than the muon chemical potential μ_μ , as shown in Fig. 2. This generates a large and positive $\mu_{a \rightarrow f}^0$ for the $a \rightarrow e^- + \mu^+$ channel, and an equally large and negative $\mu_{a \rightarrow f}^0$ for the $a \rightarrow \mu^- + e^+$ channel. This sign difference leads to an exponential suppression of the $a \rightarrow e^- + \mu^+$ decay rate relative to $a \rightarrow \mu^- + e^+$, despite the former having a larger production rate. Note that the above discussion assumes that ALPs are not in equilibrium. As we discussed previously following Eq. (4.7), in regions of parameter space where the coupling strength is sufficiently large, equilibrium between the ALP and SM particles can be achieved, leading to equal electron and muon chemical potentials. In such cases, one can no longer use the current Garching profiles. A detailed analysis of such cases will be presented in a future study [83].

5 Results

We compute the energy deposition in the SN mantle E_m via Eq. (3.1) for heavy LFV ALPs with masses $m_a > m_\mu + m_e$. In this mass regime, we consider only the dominant production process through the e - μ coalescence and the primary reabsorption term for the ALP decay process. By requiring the energy deposition in the SN mantle to be less than the LESN explosion energy, $E_m \leq 0.1$ B, we derive the constraints on the LFV ALPs.

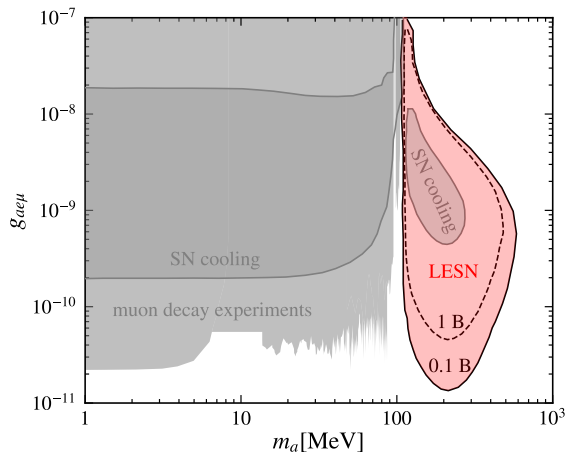


Figure 6. The LESN constraints on LFV ALPs (red-shaded region) for $E_m \leq 0.1$ B (solid). The case of $E_m \leq 1$ B (dashed) is also shown. Gray regions are the SN cooling constraints [41], and constraints from rare muon decay experiments [26, 27, 29, 30, 33], which are taken from Ref. [41].

Fig. 6 shows the LESN constraints on LFV ALPs with the requirement of $E_m \leq 0.1$ B, along with other existing experimental constraints, including those that arise from the rare muon decay experiments [26, 27, 29, 30, 33], and SN cooling limits [41]. For ALPs with masses $m_a \lesssim 105$ MeV, the SN cooling limits are primarily due to two ALP production channels in the SN core: muon decay and axion bremsstrahlung. For ALPs with masses $m_a \gtrsim 105$ MeV, the dominant ALP production channel in the SN core is the electron-muon coalescence [41]. For $m_a \lesssim 105$ MeV, the most stringent limits arise from the rare muon decay experiments, which are stronger than SN cooling limits. For $m_a \gtrsim 105$ MeV, the previously most important constraints came from SN cooling limits, where rare muon decay

experiments are kinematically forbidden. In Fig. 6, we also show the LESN constraints for the energy deposition of $E_m \leq 1$ B, which provide weaker limits than the case of $E_m \leq 0.1$ B.

We find that LESN constraints provide the most stringent constraints in the ALP mass range $m_a \sim (110, 550)$ MeV, extending the parameter space excluded by the SN cooling constraints [41] to a much larger exclusion region. In particular, the LESN constraints probe the coupling $g_{ae\mu}$ down to $\sim 10^{-11}$ for $m_a \approx 200$ MeV, which is one order of magnitude stronger than the SN cooling constraints given by Ref. [41]. Note that the LESN constraints are manifested as an exclusion region, where the upper boundary arises from significant reabsorption effects at strong couplings, while the lower boundary results from suppressed ALP production at weak couplings. Also note that for $m_a \leq 105$ MeV, ALP production through electron-muon coalescence becomes kinematically forbidden so that the low-mass region is not accessible via electron-muon coalescence in this analysis.

6 Conclusion

In this paper, we compute the LESN constraints on LFV ALPs with masses $m_a > m_\mu + m_e$, by requiring the energy deposition in the SN mantle to be less than the LESN explosion energy 0.1 B. For this mass range, we consider the dominant ALP production channel through the e - μ coalescence process [41] and the subsequent energy deposition from ALP decay. We find that the LESN constraints probe a much larger parameter space than the SN cooling limits, extending to the previously unexplored parameter space for ALP masses between 110 MeV and 550 MeV.

Acknowledgments

We thank Changqian Li, Yonglin Li, Wenxi Lu, and Zicheng Ye for discussions. We thank Hans-Thomas Janka for providing the SN profiles used for numerical calculations. The work is supported in part by the National Natural Science Foundation of China under Grant No. 12275128.

References

- [1] R. D. Peccei and H. R. Quinn, “CP Conservation in the Presence of Instantons,” *Phys. Rev. Lett.* **38** (1977) 1440–1443.
- [2] R. D. Peccei and H. R. Quinn, “Constraints Imposed by CP Conservation in the Presence of Instantons,” *Phys. Rev. D* **16** (1977) 1791–1797.
- [3] F. Wilczek, “Problem of Strong P and T Invariance in the Presence of Instantons,” *Phys. Rev. Lett.* **40** (1978) 279–282.
- [4] S. Weinberg, “A New Light Boson?” *Phys. Rev. Lett.* **40** (1978) 223–226.
- [5] G. B. Gelmini and M. Roncadelli, “Left-Handed Neutrino Mass Scale and Spontaneously Broken Lepton Number,” *Phys. Lett. B* **99** (1981) 411–415.

- [6] A. Davidson and K. C. Wali, “MINIMAL FLAVOR UNIFICATION VIA MULTIGENERATIONAL PECCEI-QUINN SYMMETRY,” *Phys. Rev. Lett.* **48** (1982) 11.
- [7] F. Wilczek, “Axions and Family Symmetry Breaking,” *Phys. Rev. Lett.* **49** (1982) 1549–1552.
- [8] P. Svrcek and E. Witten, “Axions In String Theory,” *JHEP* **06** (2006) 051 [[hep-th/0605206](#)].
- [9] A. A. Anselm, N. G. Uraltsev, and M. Y. Khlopov, “ $\mu \rightarrow e$ FAMILON DECAY,” *Sov. J. Nucl. Phys.* **41** (1985) 1060.
- [10] J. L. Feng, T. Moroi, H. Murayama, and E. Schnapka, “Third generation familons, b factories, and neutrino cosmology,” *Phys. Rev. D* **57** (1998) 5875–5892 [[hep-ph/9709411](#)].
- [11] M. Bauer, T. Schell, and T. Plehn, “Hunting the Flavon,” *Phys. Rev. D* **94** (2016) 056003 [[arXiv:1603.06950](#)].
- [12] Y. Ema, K. Hamaguchi, T. Moroi, and K. Nakayama, “Flaxion: a minimal extension to solve puzzles in the standard model,” *JHEP* **01** (2017) 096 [[arXiv:1612.05492](#)].
- [13] L. Calibbi, F. Goertz, D. Redigolo, R. Ziegler, and J. Zupan, “Minimal axion model from flavor,” *Phys. Rev. D* **95** (2017) 095009 [[arXiv:1612.08040](#)].
- [14] K. Choi, S. H. Im, C. B. Park, and S. Yun, “Minimal Flavor Violation with Axion-like Particles,” *JHEP* **11** (2017) 070 [[arXiv:1708.00021](#)].
- [15] M. Chala, G. Guedes, M. Ramos, and J. Santiago, “Running in the ALPs,” *Eur. Phys. J. C* **81** (2021) 181 [[arXiv:2012.09017](#)].
- [16] M. Bauer, M. Neubert, S. Renner, M. Schnubel, and A. Thamm, “The Low-Energy Effective Theory of Axions and ALPs,” *JHEP* **04** (2021) 063 [[arXiv:2012.12272](#)].
- [17] M. Endo, S. Iguro, and T. Kitahara, “Probing $e\mu$ flavor-violating ALP at Belle II,” *JHEP* **06** (2020) 040 [[arXiv:2002.05948](#)].
- [18] S. Iguro, Y. Omura, and M. Takeuchi, “Probing $\mu\tau$ flavor-violating solutions for the muon $g - 2$ anomaly at Belle II,” *JHEP* **09** (2020) 144 [[arXiv:2002.12728](#)].
- [19] H. Davoudiasl, R. Marcarelli, N. Miesch, and E. T. Neil, “Searching for flavor-violating ALPs in Higgs boson decays,” *Phys. Rev. D* **104** (2021) 055022 [[arXiv:2105.05866](#)].
- [20] K. Cheung, A. Soffer, Z. S. Wang, and Y.-H. Wu, “Probing charged lepton flavor violation with axion-like particles at Belle II,” *JHEP* **11** (2021) 218 [[arXiv:2108.11094](#)].
- [21] H. Davoudiasl, R. Marcarelli, and E. T. Neil, “Lepton-flavor-violating ALPs at the Electron-Ion Collider: a golden opportunity,” *JHEP* **02** (2023) 071 [[arXiv:2112.04513](#)].
- [22] T. Araki, K. Asai, H. Otono, T. Shimomura, and Y. Takubo, “Search for lepton flavor violating decay at FASER,” *JHEP* **01** (2023) 145 [[arXiv:2210.12730](#)].
- [23] L. Calibbi, Z. Huang, S. Qin, Y. Yang, and X. Yin, “Testing axion couplings to leptons in Z decays at future e^+e^- colliders,” *Phys. Rev. D* **108** (2023) 015002 [[arXiv:2212.02818](#)].
- [24] B. Batell, H. Davoudiasl, R. Marcarelli, E. T. Neil, and S. Trojanowski, “Lepton-Flavor-Violating ALP Signals with TeV-Scale Muon Beams.” [arXiv:2407.15942](#).
- [25] L. Calibbi, T. Li, L. Mukherjee, and Y. Yang, “Probing ALP Lepton Flavour Violation at μ TRISTAN.” [arXiv:2406.13234](#).
- [26] S. E. Derenzo, “Measurement of the low-energy end of the mu-plus decay spectrum,” *Phys. Rev.* **181** (1969) 1854–1866.

- [27] A. Jodidio *et al.*, “Search for Right-Handed Currents in Muon Decay,” *Phys. Rev. D* **34** (1986) 1967. [Erratum: *Phys.Rev.D* 37, 237 (1988)].
- [28] D. A. Bryman and E. T. H. Clifford, “EXOTIC MUON DECAY $\mu \rightarrow e \chi$,” *Phys. Rev. Lett.* **57** (1986) 2787.
- [29] R. Bilger *et al.*, “Search for exotic muon decays,” *Phys. Lett. B* **446** (1999) 363–367 [[hep-ph/9811333](#)].
- [30] **TWIST** Collaboration, “Search for two body muon decay signals,” *Phys. Rev. D* **91** (2015) 052020 [[arXiv:1409.0638](#)].
- [31] M. Bauer, M. Neubert, S. Renner, M. Schnubel, and A. Thamm, “Axionlike Particles, Lepton-Flavor Violation, and a New Explanation of a_μ and a_e ,” *Phys. Rev. Lett.* **124** (2020) 211803 [[arXiv:1908.00008](#)].
- [32] C. Cornella, P. Paradisi, and O. Sumensari, “Hunting for ALPs with Lepton Flavor Violation,” *JHEP* **01** (2020) 158 [[arXiv:1911.06279](#)].
- [33] **PIENU** Collaboration, “Improved search for two body muon decay $\mu^+ \rightarrow e^+ X_H$,” *Phys. Rev. D* **101** (2020) 052014 [[arXiv:2002.09170](#)].
- [34] P. Escribano and A. Vicente, “Ultralight scalars in leptonic observables,” *JHEP* **03** (2021) 240 [[arXiv:2008.01099](#)].
- [35] L. Calibbi, D. Redigolo, R. Ziegler, and J. Zupan, “Looking forward to lepton-flavor-violating ALPs,” *JHEP* **09** (2021) 173 [[arXiv:2006.04795](#)].
- [36] M. Bauer, M. Neubert, S. Renner, M. Schnubel, and A. Thamm, “Flavor probes of axion-like particles,” *JHEP* **09** (2022) 056 [[arXiv:2110.10698](#)].
- [37] S. Knapen, T. Opferkuch, D. Redigolo, and M. Tamaro, “Displaced Searches for Axion-Like Particles and Heavy Neutral Leptons at Mu3e.” [arXiv:2410.13941](#).
- [38] Y. Jho, S. Knapen, and D. Redigolo, “Lepton-flavor violating axions at MEG II,” *JHEP* **10** (2022) 029 [[arXiv:2203.11222](#)].
- [39] S. Knapen, K. Langhoff, T. Opferkuch, and D. Redigolo, “A Robust Search for Lepton Flavour Violating Axions at Mu3e.” [arXiv:2311.17915](#).
- [40] H.-Y. Zhang, R. Hagimoto, and A. J. Long, “Neutron star cooling with lepton-flavor-violating axions,” *Phys. Rev. D* **109** (2024) 103005 [[arXiv:2309.03889](#)].
- [41] Y. Li and Z. Liu, “Supernova constraints on lepton flavor violating ALPs.” [arXiv:2501.12075](#).
- [42] N. N. Chugai and V. P. Utrobin, “The nature of sn 1997d: low mass progenitor and weak explosion,” *Astron. Astrophys.* **354** (2000) 557 [[astro-ph/9906190](#)].
- [43] A. Pastorello *et al.*, “Low luminosity type II supernovae: spectroscopic and photometric evolution,” *Mon. Not. Roy. Astron. Soc.* **347** (2004) 74 [[astro-ph/0309264](#)].
- [44] A. Pastorello *et al.*, “SN 2005cs in M51 II. Complete Evolution in the Optical and the Near-Infrared,” *Mon. Not. Roy. Astron. Soc.* **394** (2009) 2266 [[arXiv:0901.2075](#)].
- [45] S. Spiro, *et al.*, “Low luminosity Type II supernovae – II. Pointing towards moderate mass precursors,” *Monthly Notices of the Royal Astronomical Society* **439** (2014) 2873–2892.
- [46] O. Pejcha and J. L. Prieto, “On The Intrinsic Diversity of Type II-Plateau Supernovae,” *Astrophys. J.* **806** (2015) 225 [[arXiv:1501.06573](#)].

- [47] H. Yang and R. A. Chevalier, “Evolution of the Crab nebula in a low energy supernova,” *Astrophys. J.* **806** (2015) 153 [[arXiv:1505.03211](#)].
- [48] M. L. Pumo, *et al.*, “Radiation-hydrodynamical modelling of underluminous type II plateau Supernovae,” *Mon. Not. Roy. Astron. Soc.* **464** (2017) 3013–3020 [[arXiv:1610.02981](#)].
- [49] J. W. Murphy, Q. Mabanta, and J. C. Dolence, “A Comparison of Explosion Energies for Simulated and Observed Core-Collapse Supernovae,” *Mon. Not. Roy. Astron. Soc.* **489** (2019) 641–652 [[arXiv:1904.09444](#)].
- [50] A. Burrows and D. Vartanyan, “Core-Collapse Supernova Explosion Theory,” *Nature* **589** (2021) 29–39 [[arXiv:2009.14157](#)].
- [51] S. Yang *et al.*, “A low-energy explosion yields the underluminous Type IIP SN 2020cxd,” *Astron. Astrophys.* **655** (2021) A90 [[arXiv:2107.13439](#)].
- [52] R. S. Teja, *et al.*, “SN 2021wvw: A core-collapse supernova at the sub-luminous, slower, and shorter end of Type IIPs.” [arXiv:2407.13207](#).
- [53] F. S. Kitaura, H.-T. Janka, and W. Hillebrandt, “Explosions of O-Ne-Mg cores, the Crab supernova, and subluminous type II-P supernovae,” *Astron. Astrophys.* **450** (2006) 345–350 [[astro-ph/0512065](#)].
- [54] T. Fischer, S. C. Whitehouse, A. Mezzacappa, F. K. Thielemann, and M. Liebendorfer, “Protoneutron star evolution and the neutrino driven wind in general relativistic neutrino radiation hydrodynamics simulations,” *Astron. Astrophys.* **517** (2010) A80 [[arXiv:0908.1871](#)].
- [55] T. Melson, H.-T. Janka, and A. Marek, “Neutrino-driven supernova of a low-mass iron-core progenitor boosted by three-dimensional turbulent convection,” *Astrophys. J. Lett.* **801** (2015) L24 [[arXiv:1501.01961](#)].
- [56] D. Radice, A. Burrows, D. Vartanyan, M. A. Skinner, and J. C. Dolence, “Electron-Capture and Low-Mass Iron-Core-Collapse Supernovae: New Neutrino-Radiation-Hydrodynamics Simulations,” *Astrophys. J.* **850** (2017) 43 [[arXiv:1702.03927](#)].
- [57] S. M. Lisakov, L. Dessart, D. J. Hillier, R. Waldman, and E. Livne, “Progenitors of low-luminosity Type II-Plateau supernovae,” *Mon. Not. Roy. Astron. Soc.* **473** (2018) 3863–3881 [[arXiv:1709.08673](#)].
- [58] B. Müller, *et al.*, “Three-Dimensional Simulations of Neutrino-Driven Core-Collapse Supernovae from Low-Mass Single and Binary Star Progenitors,” *Mon. Not. Roy. Astron. Soc.* **484** (2019) 3307–3324 [[arXiv:1811.05483](#)].
- [59] A. Burrows, D. Radice, and D. Vartanyan, “Three-dimensional supernova explosion simulations of 9-, 10-, 11-, 12-, and 13- M_{\odot} stars,” *Mon. Not. Roy. Astron. Soc.* **485** (2019) 3153–3168 [[arXiv:1902.00547](#)].
- [60] G. Stockinger *et al.*, “Three-dimensional Models of Core-collapse Supernovae From Low-mass Progenitors With Implications for Crab,” *Mon. Not. Roy. Astron. Soc.* **496** (2020) 2039–2084 [[arXiv:2005.02420](#)].
- [61] S. Zha, E. P. O’Connor, S. M. Couch, S.-C. Leung, and K. Nomoto, “Hydrodynamic simulations of electron-capture supernovae: progenitor and dimension dependence,” *Mon. Not. Roy. Astron. Soc.* **513** (2022) 1317–1328 [[arXiv:2112.15257](#)].
- [62] A. Caputo, H.-T. Janka, G. Raffelt, and E. Vitagliano, “Low-Energy Supernovae Severely

- Constrain Radiative Particle Decays,” *Phys. Rev. Lett.* **128** (2022) 221103 [[arXiv:2201.09890](#)].
- [63] G. G. Raffelt, *Stars as laboratories for fundamental physics: The astrophysics of neutrinos, axions, and other weakly interacting particles*. 1996.
- [64] S. W. Falk and D. N. Schramm, “Limits From Supernovae on Neutrino Radiative Lifetimes,” *Phys. Lett. B* **79** (1978) 511.
- [65] A. Sung, H. Tu, and M.-R. Wu, “New constraint from supernova explosions on light particles beyond the Standard Model,” *Phys. Rev. D* **99** (2019) 121305 [[arXiv:1903.07923](#)].
- [66] A. Lella, E. Ravensburg, P. Carena, and M. C. D. Marsh, “Supernova limits on ‘QCD axion-like particles.’” [arXiv:2405.00153](#).
- [67] J. Alda, G. Levati, P. Paradisi, S. Rigolin, and N. Selimovic, “Collider and astrophysical signatures of light scalars with enhanced τ couplings.” [arXiv:2407.18296](#).
- [68] G. Chauhan, S. Horiuchi, P. Huber, and I. M. Shoemaker, “Low-Energy Supernovae Bounds on Sterile Neutrinos.” [arXiv:2309.05860](#).
- [69] G. Chauhan, S. Horiuchi, P. Huber, and I. M. Shoemaker, “Probing the sterile neutrino dipole portal with SN1987A and low-energy supernovae,” *Phys. Rev. D* **110** (2024) 015007 [[arXiv:2402.01624](#)].
- [70] P. Carena, G. Lucente, L. Mastrototaro, A. Mirizzi, and P. D. Serpico, “Comprehensive constraints on heavy sterile neutrinos from core-collapse supernovae,” *Phys. Rev. D* **109** (2024) 063010 [[arXiv:2311.00033](#)].
- [71] D. F. G. Fiorillo and E. Vitagliano, “Self-interacting dark sectors in supernovae are fluid.” [arXiv:2404.07714](#).
- [72] C. Li, Z. Liu, W. Lu, and Z. Ye, “Low-Energy Supernova Constraints on Millicharged Particles.” [arXiv:2408.04953](#).
- [73] D. F. G. Fiorillo, T. Pitik, and E. Vitagliano, “Energy transfer by feebly interacting particles in supernovae: the trapping regime.” [arXiv:2503.13653](#).
- [74] G. Raffelt and D. Seckel, “Bounds on Exotic Particle Interactions from SN 1987a,” *Phys. Rev. Lett.* **60** (1988) 1793.
- [75] G. Lucente and P. Carena, “Supernova bound on axionlike particles coupled with electrons,” *Phys. Rev. D* **104** (2021) 103007 [[arXiv:2107.12393](#)].
- [76] R. Z. Ferreira, M. C. D. Marsh, and E. Müller, “Strong supernovae bounds on ALPs from quantum loops,” *JCAP* **11** (2022) 057 [[arXiv:2205.07896](#)].
- [77] “Garching core-collapse supernova research archive.” <https://wwwmpa.mpa-garching.mpg.de/ccsnarchive/>.
- [78] R. Bollig, W. DeRocco, P. W. Graham, and H.-T. Janka, “Muons in Supernovae: Implications for the Axion-Muon Coupling,” *Phys. Rev. Lett.* **125** (2020) 051104 [[arXiv:2005.07141](#)]. [Erratum: *Phys.Rev.Lett.* 126, 189901 (2021)].
- [79] H. T. Janka, B. Mueller, F. S. Kitaura, and R. Buras, “Dynamics of shock propagation and nucleosynthesis conditions in O-Ne-Mg core supernovae,” *Astron. Astrophys.* **485** (2008) 199 [[arXiv:0712.4237](#)].

- [80] L. Hudepohl, B. Muller, H. T. Janka, A. Marek, and G. G. Raffelt, “Neutrino Signal of Electron-Capture Supernovae from Core Collapse to Cooling,” *Phys. Rev. Lett.* **104** (2010) 251101 [[arXiv:0912.0260](#)]. [Erratum: *Phys.Rev.Lett.* 105, 249901 (2010)].
- [81] R. Glas, O. Just, H. T. Janka, and M. Obergaulinger, “Three-dimensional Core-collapse Supernova Simulations with Multidimensional Neutrino Transport Compared to the Ray-by-ray-plus Approximation,” *Astrophys. J.* **873** (2019) 45 [[arXiv:1809.10146](#)].
- [82] E. Braaten, “Neutrino emissivity of an ultrarelativistic plasma from positron and plasmino annihilation,” *apj* **392** (1991) 70.
- [83] Z. Huang and Z. Liu, In preparation (unpublished).